Available online at www.sciencedirect.com
ScienceDirect
Acta Materialia 55 (2007) 4867–4876
Acta MATERIALIA
www.elsevier.com/locate/actamat

Inter-martensitic transitions in Ni–Fe–Ga single crystals

R.F. Hamilton [a], H. Sehitoglu [a,*], C. Efstathiou [a], H.J. Maier [b]

[a] University of Illinois, Department of Mechanical Science and Engineering, 1206 W. Green Street, Urbana, IL 61801, USA
[b] University of Paderborn, Lehrstuhl f. Werkstoffkunde, D-33095 Paderborn, Germany

Received 23 February 2007; received in revised form 1 May 2007; accepted 6 May 2007
Available online 26 June 2007

Abstract

The strain–temperature response of Ni–Fe–Ga single crystals underscores the role of the inter-martensitic transformation in creating intersecting heating and cooling segments; the separation of these segments occurs due to irreversibilities at high stresses and at high temperatures. An ultra-narrow tensile (1 °C) and compressive (<10 °C) thermal hysteresis are observed for the $A \rightleftharpoons 10M \rightleftharpoons 14M$ case, accompanied by a small stress hysteresis (<30 MPa) in compressive and tensile stress–strain responses. The hysteresis levels increase and the intersecting segments disappear at high stresses and at high temperatures. This paper reports the use of a thermo-mechanical formulation to rationalize the role of inter-martensitic transformations. Plotting the transformation stress as a function of temperature indicates that inter-martensitic transformations enable a very wide pseudoelastic temperature range, as high as 425 °C. The measured Clausius–Clapeyron curve slope in compression (2.75 MPa $°C^{-1}$) is eight times the tensile slope (0.36 MPa $°C^{-1}$); the higher slope is attributed to the predominance of $A \rightleftharpoons L1_0$ at high temperatures.

Keywords: Martensitic transformation; Metastable phases; Tension; Compression; Hysteresis

1. Introduction

Research on the thermally induced (with no external stress) martensitic transformation (MT) in Ni–Fe–Ga alloys has shown that [1–7] the austenite exhibits $L2_1$ atomic order (Fig. 1) and transforms to martensite phases designated $10M$ or $14M$ (describing 5 and 7 modulation periods). The martensitic phases undergo the inter-martensitic transitions $A \rightleftharpoons 10M \rightleftharpoons 14M \rightleftharpoons L1_0$ or $A \rightleftharpoons 14M \rightleftharpoons L1_0$ under applied compressive or tensile stress [8,9], with the $L1_0$ structure exclusively stress-induced in this class of alloys. The $L1_0$ martensite exhibits a tetragonal structure without modulation and is illustrated in Fig. 1 along with the lattice correspondence to the $L2_1$ structure. Fig. 2 demonstrates the modulated martensitic phases composed of unit cells with monoclinic crystal structures. Although the inter-martensitic transformations have been reported, their influence on the strain–temperature (ε–T) response and asymmetric stress–strain (σ–ε) behavior is lacking. We have undertaken an extensive experimental program, including compressive and tensile ε–T and σ–ε results, microstructural interrogations and differential scanning calorimetry (DSC), to shed light on the conditions under which inter-martensitic transformations change the thermal hysteresis, the transformation temperatures, and the stress and strain levels.

The current work is the first investigation into the influence of external stress on the inter-martensitic transitions during temperature cycling, i.e. the ε–T response. To investigate transformations via the ε–T response, we raise the iso-stress levels during temperature cycling to study the progression of transformation strains, martensite and austenite start (M_s/A_s) and finish (M_f/A_f) temperatures, and thermal hysteresis. For the current $Ni_{54}Fe_{19}Ga_{27}$ alloy, the thermally induced martensite exhibits the $10M$ structure (Fig. 3a). The inset figures in Figs. 4a and 5 respec-

* Corresponding author.
E-mail address: huseyin@uiuc.edu (H. Sehitoglu).

1359-6454/$30.00 © 2007 Published by Elsevier Ltd on behalf of Acta Materialia Inc.
doi:10.1016/j.actamat.2007.05.003

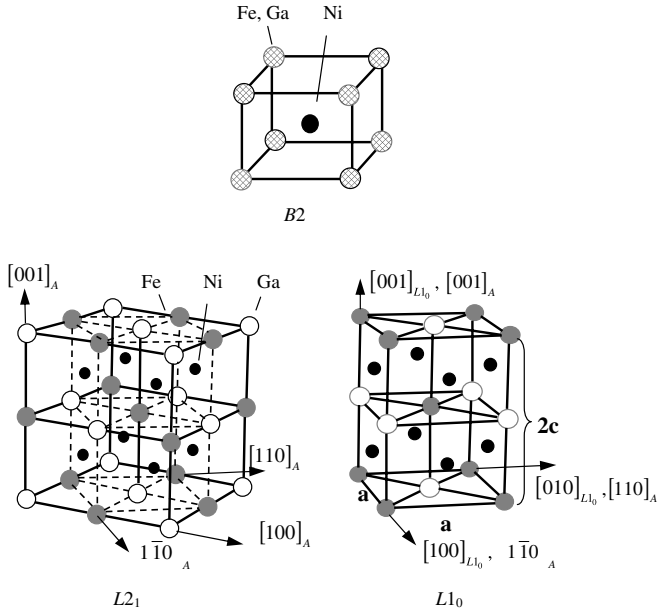

Fig. 1. $B2$ unit cell (top) exhibiting nearest-neighbor order with Fe or Ga atoms occupying the corner positions. When $L2_1$ order (lower left) is achieved, nearest- and next-nearest-neighbor order exists; Fe and Ga atoms occupy specific corner positions and Ni atoms remain at the center. The dashed lines illustrate the correspondence between the lattice and the face-centered tetragonal (fct) $L1_0$ structure shown to the right.

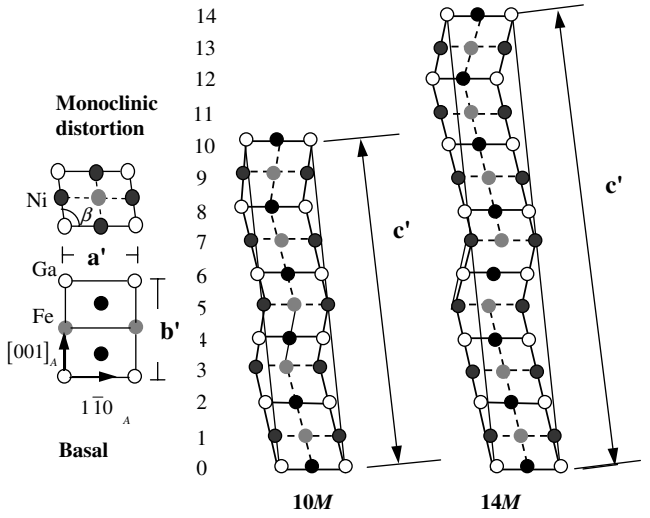

Fig. 2. Schematic representations of the $10M$ and $14M$ modulated martensite phases. The unit cells exhibit a monoclinic distortion defined by the angle β; $\mathbf{a}'$, $\mathbf{b}'$ and $\mathbf{c}'$ are the lattice parameters. For the modulated phase, the basal plane is spanned by $[1\,\bar{1}\,0]_A$ and $[0\,0\,1]_A$ and the planes are stacked along the $[1\,1\,0]_A$ direction. For the modulated phases, the basal planes are shuffled along the $[1\,\bar{1}\,0]_A$ direction. The shuffling is repeated every five planes to produce the $10M$ phase and every seven planes to produce the $14M$ phase.

tively illustrate the tensile and compressive ε–T responses for $A \rightleftharpoons 10M$ and $A \rightleftharpoons 10M \rightleftharpoons 14M$. For the inter-martensitic transformation $A \rightleftharpoons 10M \rightleftharpoons 14M$, the principal findings are that the A_s temperature is below M_s, and thus $\Delta T_s = A_s - M_s < 0$, and that the heating and cooling segments intersect. In compression, A_s nears M_f and then the segments intersect. We derive an expression for $\Delta T_s = A_s - M_s$ from a thermo-mechanical formulation justifying $\Delta T_s < 0$.

Our preliminary work [10] on the σ–ε response in $\langle 0\,0\,1\rangle$ and $\langle 1\,2\,3\rangle$ oriented single crystals investigated asymmetry at temperatures within the range of $-50\,^{\circ}\mathrm{C} \leqslant T \leqslant 75\,^{\circ}\mathrm{C}$. For the current study, we focus on the $\langle 0\,0\,1\rangle$ orientation because large recoverable strains occur with limited slip deformation effects. Building on our previous study, the σ–ε response is evaluated at $T = A_f + 25\,^{\circ}\mathrm{C}$ up to temperatures as high as 450 °C, revealing that inter-martensitic transformations allow very high-temperature intervals (up to 425 °C) for pseudoelasticity. Applied strains as high as +12% and −6% are completely recoverable with the drastic asymmetry attributed to considerable detwinning strain for the $L1_0$ structure, which can reach +8.2% based on theoretical predictions. The σ–ε response as the temperature is elevated reveals that the intermediate $A \rightleftharpoons 10M$ transformation is bypassed with increasing transformation stress.

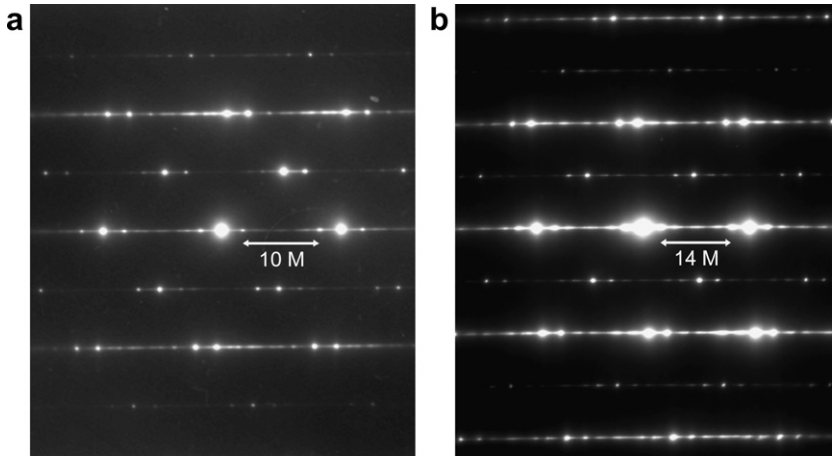

Fig. 3. SAD patterns of martensite phases exhibiting (a) $10M$ and (b) $14M$ modulated structures. The $10M$ martensite (a) is thermally induced from austenite without applied stress. The $14M$ martensite (b) is stress-induced during thermal cycling under constant tensile stress.

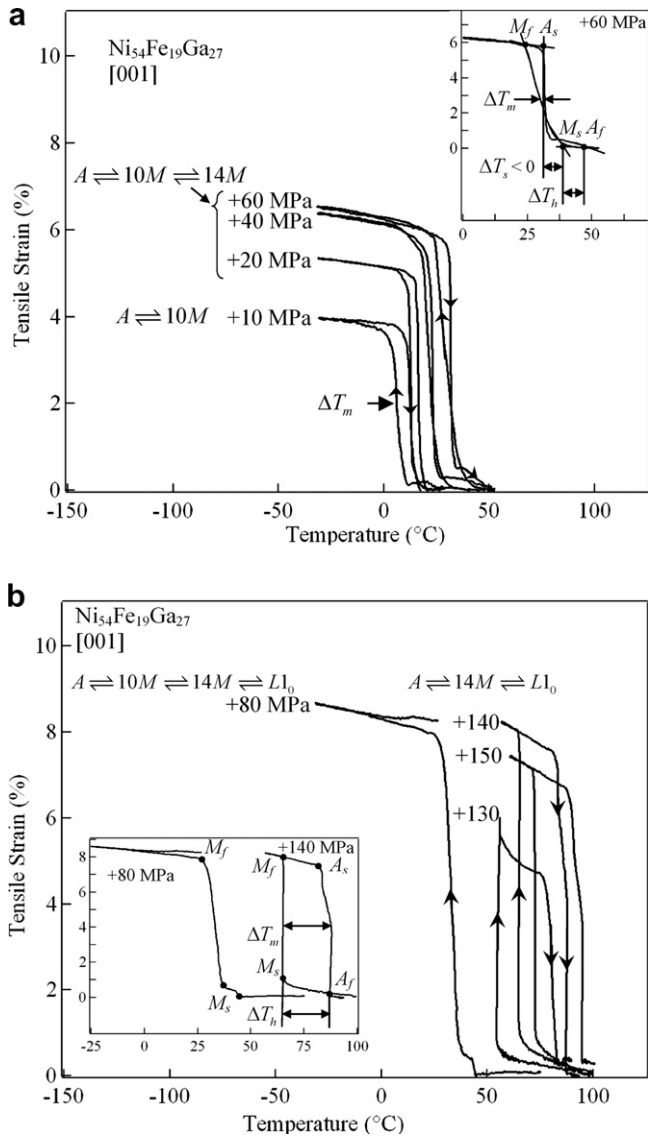

Fig. 4. The tensile strain–temperature response as the iso-stress increases, culminating in the formation of (a) $14M$ and (b) $L1_0$ martensite structures. The transformation steps are rationalized in the text. Arrows along the curves indicate directions of cooling and heating. (a) The heating and cooling segments intersect in the inset. The characteristic temperatures (M_s, M_f, A_s, A_f) are determined by the method of intersecting slopes. When the transformation steps are $A \rightleftharpoons 10M \rightleftharpoons 14M$, the A_s temperature is lower than M_s and $\Delta T_s = A_s - M_s < 0$. Thermal hysteresis $\Delta T_h = A_f - M_s = 7\ ^\circ C$; however, the hysteresis measured at the mid-strain ΔT_m is nearly 1 °C. (b) The specimens fail in the range +80 to +120 MPa. At +130 MPa, the transformation and strains are completely recovered because the transformation changes to $A14 \rightleftharpoons M \rightleftharpoons L1_0$. For this transformation, $A_s > M_s$ and $\Delta T_s > 0$ and the thermal hysteresis $\Delta T_h = \Delta T_m$ widens considerably (inset (b)).

Accordingly, the transformation steps in tension evolve from $A \rightleftharpoons 10M \rightleftharpoons 14M \rightleftharpoons L1_0$ to $A \rightleftharpoons 14M \rightleftharpoons L1_0$; whereas, in compression, the steps evolve from $A \rightleftharpoons 10M \rightleftharpoons 14M$ to $A \rightleftharpoons 14M \rightleftharpoons L1_0$ to $A \rightleftharpoons L1_0$. Due to the contrasts, the Clausius–Clapeyron (C–C) relationship exhibits a striking asymmetry and the slope in compression (2.75 MPa $^\circ C^{-1}$) is nearly eight times that in tension (0.36 MPa $^\circ C^{-1}$).

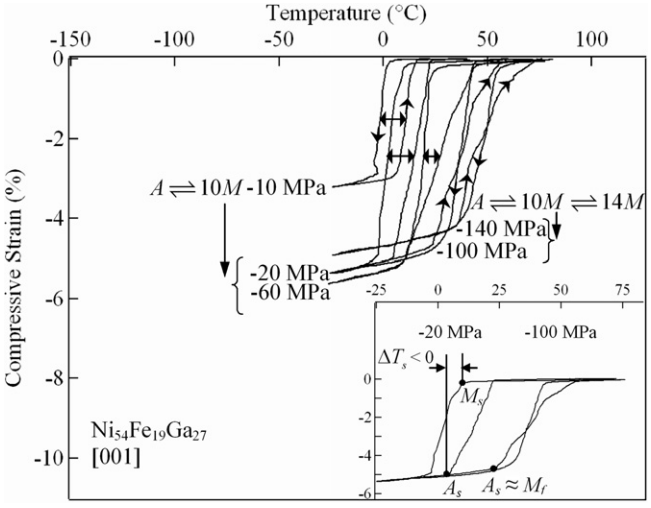

Fig. 5. The compressive strain–temperature response as the iso-stress increases. The transformation steps are described in more detail in the text. In the inset figure, the transformation facilitates $\Delta T_s < 0$, and the heating and cooling strain–temperature curves intersect. Therefore, the transformation steps $A \rightleftharpoons 10M \rightleftharpoons 14M$ are the same as Fig. 4a. The caption of that figure explains the notation here. $A_s \approx M_f$ at −60 MPa and the heating and cooling curves overlap. When the MT $A \rightleftharpoons 14M$ is facilitated at −90, −100, −140 MPa, the curves intersect (inset).

The inter-martensitic transformation $A \rightleftharpoons 10M \rightleftharpoons 14M$ facilitates a small thermal hysteresis $\Delta T_h = A_f - M_s$ (<6 °C) and the heating and cooling segments intersect (Fig. 4a inset). In the absence of inter-martensitic transformations the heating and cooling segments do not intersect. Remarkably, the thermal hysteresis ΔT_m, measured at half the recoverable strain (Fig. 4a), shrinks to as low as ~1 °C. We note that enhanced elastic strain energy storage related to the inter-martensitic transformation enables the tiny ΔT_m. Inter-martensitic transformation alone does not guarantee a low hysteresis level. For $A \rightleftharpoons 14M \rightleftharpoons L1_0$, operating high above austenite finish temperature and at high stresses, the hysteresis is significantly wider, indicating that irreversiblities are severe. The stress hysteresis $\Delta\sigma_h = \Sigma_F - \Sigma_R$ is measured as the difference between the forward Σ_F and reverse Σ_R transformation stresses. Analogous to the thermal hysteresis, $\Delta\sigma_h$ is small in tension (20 MPa) and compression (26 MPa) for $A \rightleftharpoons 10M \rightleftharpoons 14M$, and grows when $A \rightleftharpoons 14M \rightleftharpoons L1_0$ is stress-induced. We derive expressions for ΔT_h and $\Delta\sigma_h$ and explain the narrow hysteresis for $A \rightleftharpoons 10M \rightleftharpoons 14M$ and the wider hysteresis for $A \rightleftharpoons 14M \rightleftharpoons L1_0$.

2. Materials and methods

The alloy was cast to a nominal composition of $Ni_{54}Fe_{19}Ga_{27}$ (at.%). Single crystal ingots were grown using the Bridgman technique in an inert environment. Compression (4 mm × 4 mm × 10 mm) and dog-bone tension (3 mm × 1.5 mm × 1.3 mm gauge section) specimens were electro-discharge machined from the ingot in the desired single crystal orientations. From our previous

work [10], the transformation temperatures are $M_s = 6$ °C, $M_f = -8$ °C, $A_s = 9$ °C and $A_f = 24.4$ °C. Transmission electron microscopy (TEM) analysis was performed to resolve microstructural features using high magnifications. A selected area diffraction (SAD) pattern exposing the stress-free, thermally induced $10M$ martensite is shown in Fig. 3a. Fig. 3b shows the SAD pattern of stress-induced $14M$ martensite retained after thermal cycling under load.

Uniaxial compression and tension loads were applied using a servo-hydraulic load frame, and strain was measured via a miniature extensometer with a 3 mm gauge length. Isothermal strain cycling experiments in the temperature range of 25–440 °C were conducted from ±2% up to maximum strain levels as high as +12% and −6%. The transformation stress was measured using the 0.2% offset method. In cases where the strain was not fully recovered upon unloading, the specimens were heated to recover the strain via the shape memory effect. A second set of experiments was performed under constant tensile and compressive applied stress (iso-stress) while cycling the temperature. The iso-stresses were increased from ±10 MPa up to the maximum load at which gross plastic deformation was observed.

3. Theoretical modeling

3.1. Transformation strains

We calculate the theoretical transformation strain for a correspondence variant pair (CVP) using a framework called the "energy minimization theory" (EMT) [11]. Two martensite variants twinned to one another constitute a CVP. The twin parameters within the CVP and the CVP habit (invariant) plane orientations and transformation directions are determined for Ni–Fe–Ga with the lattice parameters [8] $a_0 = 2.88$Å for the $B2$ austenite, and $c = 3.27$Å, and $a = 3.81$Å for the $L1_0$ martensite. Note the lattice parameter $2a_0 = 5.76$ Å when the austenite achieves the $L2_1$ ordered supercell in Fig. 1; similarly the tetragonal axis is $2c$ in Fig. 1. Based on the EMT, the twin plane and twin shear vectors were calculated $\boldsymbol{n} = \{-1\,1, 0\}$, and $\boldsymbol{a} = \langle 0, 0.2531, 0.3072\rangle$; the habit plane normal and transformation directions were also calculated $\boldsymbol{m} = \{-0.7027, 0.1014, 0.7042\}$ and $\boldsymbol{b} = \langle 0.0945, 0.0120, 0.0834\rangle$. To establish the overall transformation strains, including CVP formation and detwinning of a CVP (i.e. a single variant martensite plate), we employ the lattice deformation theory (LDT) [12]. A more detailed discussion of these calculations can be found in the references, and Table 1 shows the results for the structural transformation to $L1_0$. For the tensile loading direction, the detwinning contribution is 8.2%; whereas this contribution is negligible in compression. The published theoretical tensile strains for the monoclinic $10M$ and $14M$ structures are 4.6% and 6.2%, respectively [1]. The structures and the lattice parameters, $\mathbf{a}'$, $\mathbf{b}'$, $\mathbf{c}'$ and β are shown in Fig. 2.

Table 1
Theoretical and experimental recoverable strains for the martensitic transformation to the $L1_0$ structure

Stress state	Recoverable strain (%)			
	Theoretical ($L1_0$)		Experimental	
	CVP formation	CVP + detwinning	σ–ε	ε–T
Tension	6.3	14.5	12	9
Compression	−6.3	−6.3	−6	−5.5

For the theoretical predictions, correspondent variant pair (CVP) strain is based on the energy minimization theory and CVP + detwinning strain is based on the lattice deformation theory. The experimental strains are the maximum values measured from tensile and compressive stress–strain, σ–ε (Figs. 6 and 7), and strain–temperature, ε–T (Figs. 4b and 5) curves.

3.2. Transformation temperatures and hysteresis

The thermodynamic potential governing the MT is the complementary Gibbs free energy [13,14]. The thermodynamic driving force for transforming martensite is determined from partial differentiation of the complementary free energy with respect to the volume fraction of the nth variant, f^n, such that

$$F^n = -B(T - T_0) + \sigma_{ij}^{\text{app}}\varepsilon_{ij}^n + \frac{\partial}{\partial f^n}\left[\frac{1}{2V}\int_\Omega \sigma_{ij}^{\text{m-dist}}\varepsilon_{ij}^{\text{dist-tr}}\,\mathrm{d}V\right]. \quad (1)$$

The first term on the right-hand side of Eq. (1) represents the chemical driving force (i.e. the contribution from the atomic structure) for the transformation at temperature T. The equilibrium temperature is designated T_0 and B is a material constant equal to $|\Delta s|$, where Δs is the entropy of the transformation per unit volume and is negative and proportional to $(\varepsilon^{\text{tr}})^2$ [15]. The second term in Eq. (1) is the mechanical driving force due to the applied stress, σ_{ij}^{app}, generating the transformation strain, ε_{ij}^n, of the nth martensite variant. The last term is the energetic contribution of martensite variant interactions; hence, $\sigma_{ij}^{\text{m-dist}}$ and $\varepsilon_{ij}^{\text{dist-tr}}$ are the local disturbance stress and strain due to the transformation. This interaction energy has been shown to be a negative quantity [13], and is denoted as $W_{\text{interaction}}$ throughout this work. The chemical energy and the applied stress assist the transformation, while the interaction energy opposes it.

The hysteresis of the MT results from inherent irreversible processes. These are mainly three factors: frictional resistance to interfacial motion, interaction of differently oriented martensite variants, and plastic accommodation of the transformation strain [16]. The thermodynamic driving force on the nth CVP given by Eq. (1) must reach a critical value F_C for the transformation to occur. F_C represents the microstructure resistance to the MT and is influenced by factors that affect the yield strength, such as the degree of atomic order and the presence of inhomogeneities (i.e. precipitates, dislocations or residual martensite). When Eq. (1) is applied to a single step MT, such as $A \rightleftharpoons 10M$, the critical condition for the forward (F) and reverse (R) transformations are

$$+F_{C(F)} = B(T_0 - T) + \sigma_{ij}^{app}\varepsilon_{ij}^{n} - |W_{interaction}| \quad (2a)$$

$$-F_{C(R)} = B(T_0 - T) + \sigma_{ij}^{app}\varepsilon_{ij}^{n} - |W_{interaction}| \quad (2b)$$

Inter-martensitic transformations are stress-induced in the $Ni_{54}Fe_{19}Ga_{27}$ ⟨0 0 1⟩ single crystals (Figs. 4–8) and the transformation steps are $A \rightleftharpoons 10M \rightleftharpoons 14M$. We envisage the forward transformation to be $A \rightarrow 10M \rightarrow 14M$; once the $14M$ habit plane, i.e. the undistorted plane between austenite and $14M$, exists, untransformed austenite can transform directly to martensite, i.e. $A \rightarrow 14M$. Therefore, Eq. (2a) now applies to the forward transformation $A \rightarrow 10M$ and Eq. (2b) to the reverse one $A \leftarrow 14M$; consequently, the values of B, T_0, ε_{ij}^{n} and $W_{interaction}$ differ in the equations. The critical condition for each transformation is

$$F_{C(F)} = B_F(T_{0(F)} - T) + \sigma_{ij}^{app}\varepsilon_{ij(F)}^{n} - |W_{interaction(F)}| \quad (3a)$$

$$-F_{C(R)} = B_R(T_{0(R)} - T) + \sigma_{ij}^{app}\varepsilon_{ij(R)}^{n} - |W_{interaction(R)}| \quad (3b)$$

After rearranging Eq. (3a), the M_s temperature is

$$M_s = T_{0(F)} + \frac{\sigma_{ij}^{app}\varepsilon_{ij(F)}^{n} - F_{C(F)} - |W_{interaction(F)}|}{B_F}. \quad (4)$$

The A_s temperature is determined from a similar treatment of Eq. (3b) and

$$A_s = T_{0(R)} + \frac{\sigma_{ij}^{app}\varepsilon_{ij(R)}^{n} + F_{C(R)} - |W_{interaction(R)}|}{B_R}. \quad (5)$$

Based on Eqs. (4) and (5), and substituting $B = |\Delta s|$, the difference $\Delta T_s = A_s - M_s$ is

$$\Delta T_s = [T_{0(R)} - T_{0(F)}] + \left[\frac{\sigma_{ij}^{app}\varepsilon_{ij(R)}^{n} + F_{C(R)} - |W_{interaction(R)}|}{|\Delta s_R|} - \frac{\sigma_{ij}^{app}\varepsilon_{ij(F)}^{n} - F_{C(F)} - |W_{interaction(F)}|}{|\Delta s_F|}\right]. \quad (6)$$

The inter-martensitic transformation $A \rightleftharpoons 10M \rightleftharpoons 14M$ enables $\Delta T_s < 0$, as illustrated in the inset of Fig. 4a. Considering Eq. (6), $T_{0(R)} < T_{0(F)}$ facilitates a negative value of ΔT_s. Factors making the second bracketed term negative follow. Note that the interaction energy term will be negligible at the start of the forward MT due to the small initial volume fraction of the product phase. At the start of the reverse MT, on the other hand, substantial martensite variants exist and the interaction energy $|W_{interaction(R)}|$ *enables* $\Delta T_s < 0$. Specifically, the energy stored during the forward transformations assists the reverse transformation, reducing the chemical driving force represented as $B(T_0 - T)$ in Eq. (2b). The chemical force is $B(T_0 - A_s)$ at $T = A_s$; because the force is reduced, A_s can be driven below M_s, making $\Delta T_s < 0$. Clearly, the transformation strain for the $A \rightarrow 10M$ MT being greater than that for $A \leftarrow 14M$ ($\varepsilon_{ij(F)}^{n} > \varepsilon_{ij(R)}^{n}$) will promote $\Delta T_s < 0$. A larger entropy change for the reverse MT compared to the forward MT ($|\Delta s_R| > |\Delta s_F|$) will also promote $\Delta T_s < 0$. Note that when the inter-martensitic transformation is not encountered, $\Delta T_s > 0$ as for the $A \rightleftharpoons 10M$ case (Fig. 4a).

The temperature hysteresis is defined as $\Delta T_h = A_f - M_s$. For the $A \rightleftharpoons 10M \rightleftharpoons 14M$, the M_s temperature corresponds to $A \rightarrow 10M$ and A_f corresponds to $A \leftarrow 10M$. Therefore, the analysis is analogous to the single step MT $A \rightleftharpoons 10M$ (see Fig. 4a), and the transformation temperatures to a first approximation are determined from Eqs. (2a) and (2b), respectively and

$$\Delta T_h = A_f - M_s = (F_{C(R)} + F_{C(F)})/|\Delta s|. \quad (7)$$

The stress hysteresis is characterized by $\Delta\sigma_h = \Sigma_F - \Sigma_R$. For isothermal uniaxial loading, there will be one component of stress and strain; hence the indices are dropped in Eqs. (3a) and (3b). After rearrangement:

$$\Delta\sigma_h = \Sigma_F - \Sigma_R = \frac{1}{\varepsilon_F^{tr}}[|\Delta s_F|(T - T_{0(F)}) + F_{C(F)} + |W_{interaction(F)}|] - \frac{1}{\varepsilon_R^{tr}}[|\Delta s_R|(T - T_{0(R)}) - F_{C(R)} + |W_{interaction(R)}|] \quad (8)$$

Smaller forward transformation strains (ε_F^{tr} for $A \rightarrow 10M$) compared to reverse ones (ε_R^{tr} for $10M \leftarrow 14M$) imply $|\Delta s_R| > |\Delta s_F|$ and cause the stress hysteresis to narrow. Since the F_C terms are additive, a higher resistance leads to a wide hysteresis. For $A \rightleftharpoons 10M$, $\Sigma_{(F)}$ and $\Sigma_{(R)}$ are determined from Eqs. (2a) and (2b) and the stress hysteresis is defined as:

$$\Delta\sigma_h = \Sigma_F - \Sigma_R = (F_{C(F)} + F_{C(R)})/\varepsilon^{tr}. \quad (9)$$

Caution should be exercised when considering Eqs. (7) and (9), which imply that a large entropy change or transformation strain will facilitate a small hysteresis and vice versa. Instead, Eqs. (7)–(9) illustrate that the resistive forces, $F_{C(F)}$ and $F_{C(R)}$, dictate the hysteresis [16]. Further discussion of Eqs. (6)–(9) as they apply to inter-martensitic transformations is given in the Discussion.

4. Experimental results

4.1. Tensile strain–temperature

The tensile strain–temperature (ε–T) responses of $Ni_{54}Fe_{19}Ga_{27}$ ⟨0 0 1⟩ single crystals over a wide range of iso-stresses are summarized in Fig. 4. The MT $A \rightleftharpoons 10M$ takes place at +10 MPa, and the 4% recoverable strain (Fig. 4a) is consistent with the 4.6% theoretical strain predicted for the $10M$ structure. The strain saturates around +6.4% at +60 MPa, which compares well with the +6.2% theoretical value predicted for the $14M$ structure. We envisage that the inter-martensitic transformation $A \rightleftharpoons 10M \rightleftharpoons 14M$ takes place and the $14M$ structure becomes primary as the iso-stress increases from +20 to +60 MPa. Scrutiny of the transformation temperatures in this stress range reveals that the A_s temperature is below M_s (inset Fig. 4a) and $\Delta T_s = A_s - M_s < 0$ when $A \rightleftharpoons 10M \rightleftharpoons 14M$ is stress-induced. The measured thermal hysteresis $\Delta T_h = A_f - M_s = 7°C$ is constant from

+20 to +60 MPa. On the other hand, the thermal hysteresis ΔT_m, measured at half the recoverable strain (inset), shrinks; culminating in the striking intersection of the cooling and heating segments at +40 to +60 MPa in Fig. 4a. Multiple stages exist in the heating segment, marked by two arrows. Although stages are not evident during cooling, the slope of the segment becomes less steep as the iso-stress increases in Fig. 4a. Specifically, the temperature interval for the forward transformation ($M_s - M_f$) increases as the 14*M* structure becomes predominant.

Tensile ε–T responses at higher iso-stresses are shown in Fig. 4b. At +80 MPa, the M_s temperature is 35 °C and the tensile σ–ε response at $T = 35$ °C (Fig. 6a) shows that the inter-martensitic transformation $A \rightleftharpoons 10M \rightleftharpoons 14M \rightleftharpoons L1_0$ is stress-induced. Recoverable strain levels (+8.7%) surpass the theoretical CVP formation strain for the $L1_0$ structure in Table 1, and thus the CVPs detwin. Fracture occurs at +80 MPa and prevails until the iso-stress is +130 MPa. At +130, +140 and +150 MPa (right-hand side of Fig. 4b), the tensile σ–ε response (Fig. 6b) shows that the intermediate transition to 10*M* is bypassed and the transformation is $A \rightleftharpoons 14M \rightleftharpoons L1_0$. In the inset, ΔT_s is positive and the thermal hysteresis $\Delta T_h = \Delta T_m$ (30 °C) grows considerably compared to the hysteresis for $A \rightleftharpoons 10M \rightleftharpoons 14M$ (Fig. 4a).

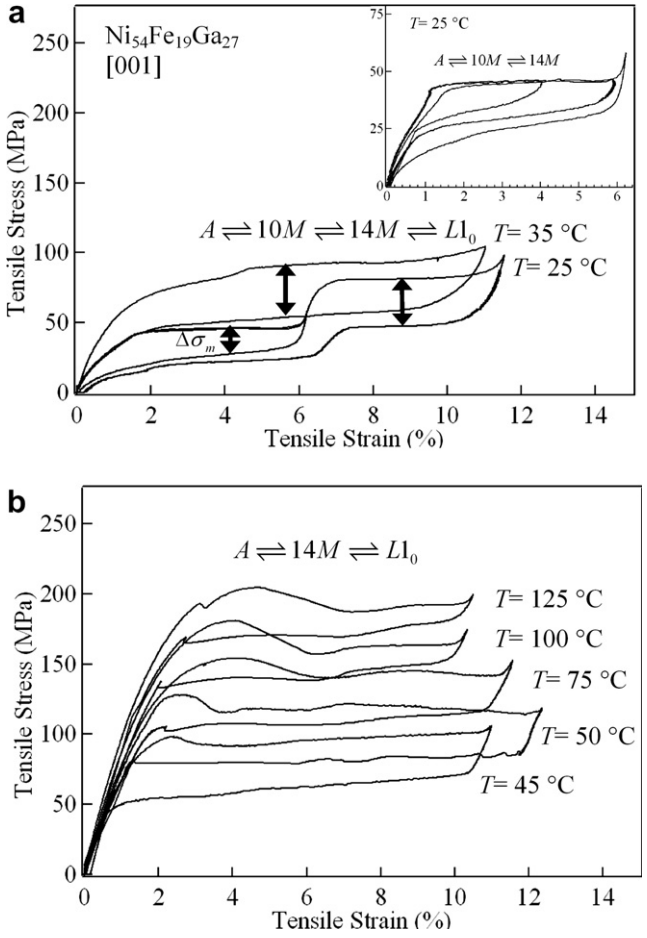

Fig. 6. The tensile stress–strain response at (a) $T = 25$ and $T = 35$ °C, and (b) as T is elevated from 45 up to 125 °C. The vertical double arrows illustrate the stress hysteresis, $\Delta\sigma_m$, defined at half the recoverable strain. The inter-martensitic transformation $A \rightleftharpoons 10M \rightleftharpoons 14M$ facilitates the non-linear response in (a) and the transformation is $14M \rightleftharpoons L1_0$ at the second stress plateau. The σ–ε response for $A \rightleftharpoons 10M \rightleftharpoons 14M$ is isolated in the inset figure. At $T = 45$ °C (b), the $A \rightleftharpoons 10M$ MT is bypassed and the loading segment is linear and the stress drops prior to a stress plateau. At $T > 50$ °C, note the recoverable strain and decrease in $\Delta\sigma_m$ with increasing temperature in (b).

4.2. Compressive strain–temperature

Representative compressive ε–T responses highlighting critical findings are included in Fig. 5. The $A \rightleftharpoons 10M$ MT occurs at −10 MPa and the $M_s = 8.6$ °C matches M_s temperatures determined from the DSC analysis and from the tensile ε–T response at +10 MPa. The $\Delta T_s = A_s - M_s < 0$ at −20 MPa (inset) and, remarkably, A_s is equal to M_f at −60 MPa. Due to the wide thermal hysteresis, ΔT_m, at −20 up to −60 MPa, and because the magnitude is close to that at −10 MPa, the martensite phase is primarily 10*M*. The hysteresis shrinks considerably as the stress is increased farther, and the heating and cooling segments intersect when $A_s \approx M_f$ (inset) at −100 MPa. The compressive σ–ε responses exhibiting comparable transformation stress ($T = 50$ °C in Fig. 7) verify the transformation is $A \rightleftharpoons 10M \rightleftharpoons 14M$ and that the 14*M* structure is predominant. In light of the tiny ΔT_m at −140 MPa, the $L1_0$ structure is not compressive stress-induced and the 10*M* structure is stable up to higher stress magnitudes.

4.3. Tensile stress–strain

To establish the pseudoelastic response in $Ni_{54}Fe_{19}Ga_{27}$ ⟨0 0 1⟩ single crystals, incremental strain cycles are con-

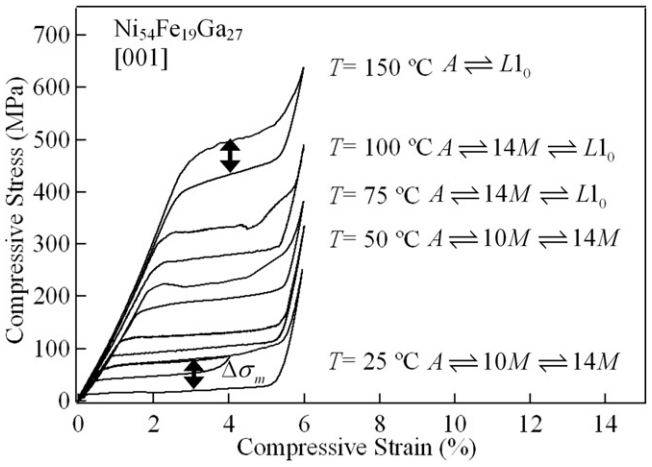

Fig. 7. The compressive stress–strain response at $T \geqslant 25$ °C. The hysteresis $\Delta\sigma_m$ is narrowest at $T = 50$ °C. Compared to tension (Fig. 6), the $A \rightleftharpoons 10M$ MT is bypassed at larger stresses. Moreover, the intermediate transformation $A \rightleftharpoons 14M$ is bypassed in compression. The findings show that the compressive transformation steps evolve with temperature at $T \geqslant 50$ °C and the hysteresis grows with increasing temperature. The temperature dependence of the transformation steps and hysteresis is explained in the text.

ducted at temperatures above the A_f temperature (24.4 °C) determined from DSC. Close to A_f, at $T = 25$ °C, the tensile σ–ε response exhibits two stress plateaus in Fig. 6a. At the first plateau (inset), +6% strain is recovered and, based on agreement with theoretical predictions, the $14M$ structure is stress-induced. The total recoverable strain is nearly 12%; therefore, at the second plateau, the detwinned $L1_0$ structure is stress-induced. A single plateau exists at $T = 35$ °C and the stress and hysteresis $\Delta\sigma_m$ compare well with those for the second stress plateau at $T = 25$ °C. The σ–ε response is noticeably non-linear at $T = 35$ and 25 °C (inset). The transformation stress at $T = 25$ and 35 °C is approximately 30 MPa. The ε–T responses at equivalent iso-stresses show that $A \rightleftharpoons 10M \rightleftharpoons 14M$ is stress-induced and probably facilitates the non-linear σ–ε response. The findings show the transformation steps are $A \rightleftharpoons 10M \rightleftharpoons 14M \rightleftharpoons L1_0$ at $T = 25$ and 35 °C.

At $T = 45$ °C, the stress reaches a maximum and drops to a plateau in Fig. 6b. A more severe drop in stress occurs at $T \geqslant 50$ °C. We propose that the intermediate transformation $A \rightleftharpoons 10M$ is bypassed, and ascribe the stress drop to the inter-martensitic transformation $A \rightleftharpoons 14M \rightleftharpoons L1_0$. In fact, the σ–ε response exhibits a stress drop prior to a plateau up to temperatures as high as 450 °C; hence $A \rightleftharpoons 14M \rightleftharpoons L1_0$ is stable. As the temperature increases above 50 °C, the recoverable strain decreases to 10.5%, implying a lower detwinning contribution. The stress hysteresis decreases noticeably, as well, which is attributed to lower levels of detwinning strain.

4.4. Compression stress–strain

The pseudoelastic σ–ε responses in compression are summarized in Fig. 7. At $T = 25$ °C, the transformation stress is −60 MPa, and the compressive ε–T response at −60 MPa shows $A \rightarrow 10M$ is primary. When −4% strain is applied, the stress increases to nearly −90 MPa, and for −6% applied strain, it increases farther to −110 MPa prior to elastic deformation of martensite. Comparing the high compressive stress levels to similar iso-stress (Fig. 5), the inter-martensitic transformation $A \rightleftharpoons 10M \rightleftharpoons 14M$ takes place and $14M$ becomes the dominant martensite structure as the stress increases above −90 MPa when −6% strain is applied. At $T = 50$ °C, the hysteresis shrinks to 28 MPa and we conclude that the pre-eminent transformation to $14M$ produces the narrow hysteresis. At $T = 75$ and 100 °C, a stress drop is evident in the σ–ε curves and the hysteresis widens to 55 MPa at $T = 100$ °C. The stress drop and hysteresis growth are attributed to the inter-martensitic transformation $A \rightleftharpoons 14M \rightleftharpoons L1_0$, similar to the tensile σ–ε response. The σ–ε curve is steeply inclined at $T = 150$ °C, which is in stark contrast to the curves at lower temperatures; hence, it is probable that the transformation is $A \rightleftharpoons L1_0$.

In Fig. 8, the transformation stress as a function of temperature is demonstrated at $T \geqslant 50$ °C. The transition from pseudoelastic behavior to slip occurs at the M_d temperature. Remarkably, the M_d temperature for tension is not observed in the temperature range. Slip takes place in compression and is related to the occurrence of $A \rightleftharpoons L1_0$. The compressive C–C slope (2.93 MPa °C^{-1}) is over 8 times that for tension (0.36 MPa °C^{-1}). In the discussion, we accredit the highly asymmetric response to the evolution of the transformation steps in compression from $A \rightleftharpoons 10M \rightleftharpoons 14M$ to $A \rightleftharpoons L1_0$.

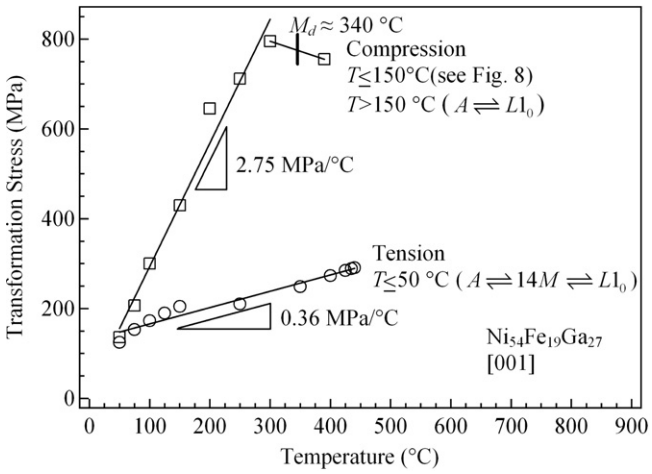

Fig. 8. The transformation stresses as function of isothermal temperature at $T \geqslant 50$ °C. The transformation steps from Figs. 6b and 7 are included and those at the highest temperatures in the figures remain the same as the temperature increases. The Clausius–Clapeyron slopes (MPa °C^{-1}) are determined from the fit lines. The striking asymmetry is attributed to the temperature-dependent transformation sequences in compression (Fig. 7) with $A \rightleftharpoons L1_0$ occurring at the highest temperature. The temperature at which the martensite is strain-induced, M_d, is evident in compression; however, it is not observed in tension.

5. Discussion

5.1. Strain–temperature

The major finding from the ε–T analysis is that the A_s temperature is below M_s, making $\Delta T_s = A_s - M_s < 0$ when the inter-martensitic transformation $A \rightleftharpoons 10M \rightleftharpoons 14M$ is stress-induced. We envisage that the austenite transforms to the intermediate $10M$ structure, which subsequently converts to $14M$. Due to the existence of the habit plane, i.e. the undistorted plane between the $L2_1$ austenite and $14M$, the remaining austenite domains can convert directly to the $14M$ structure. During the reverse transformation, a fraction of the $14M$ domains will revert directly to austenite and others will undergo $A \leftarrow 10M \leftarrow 14M$ creating multiple stages in the heating segments in Figs. 4a and 5. Therefore, the forward (F) MT in Eq. (6) refers to $A \rightarrow 10M$ and the reverse (R) MT corresponds to $A \leftarrow 14M$. According to theoretical predictions (Ref. [8] and Table 1), the tensile transformation strain $\varepsilon^n_{ij(F)} = 4.6\%$ and $\varepsilon^n_{ij(R)} = 6.2\%$. The entropy changes $|\Delta s_F|$ and $|\Delta s_R|$ are proportional to the square of the transformation strains, and thus, $|\Delta s_R| > |\Delta s_F|$ and the second bracketed term in Eq. (6) is indeed negative.

In addition to changes in entropy, the low A_s temperature is related to the elastic strain energy stored during the forward transformation. The temperature interval $M_s - M_f$ is related to the intensity of elastic strain energy; a wide interval implies significant energy is stored [16,17]. At +10 MPa, $M_s - M_f = 8$ °C and it widens to 15 °C at +60 MPa, and thus the transformation to the $14M$ structure enhances stored energy. The energy can assist the reverse transformation as $|W_{\text{interaction(R)}}|$ in Eq. (2b), facilitating a lower chemical contribution, and thus A_s shifts closer to M_f. In compression, the interval at −140 MPa is three times wider than −10 MPa. The drastic increase implies the transformation to $14M$ produces greater elastic energy storage in compression, which enables $A_s \approx M_f$.

The outstanding observation that the heating and cooling segments intersect can be understood by considering the stages during heating. The first stage occurs over a narrow temperature range (Figs. 4a and 5). Analogous to the elastic energy stored during the forward MT, the small range shows that little strain energy is released. In tension (Fig. 4a), the range is as low as 2 °C and the heating segment intersects the cooling segment. The second stage ($A \leftarrow 10M \leftarrow 14M$) proceeds over a broader temperature interval, implying that more strain energy is released. In Fig. 4a, the heating segment intersects the cooling one again in tension. In compression, $A \leftarrow 10M \leftarrow 14M$ occurs over a much broader temperature interval and considerable strain is recovered as the heating segment intersects the cooling one in Fig. 5. Ultimately, the reverse temperature range is widest, proving that more elastic energy is released, and consequently stored, in compression. The findings confirm that considerable elastic strain energy is stored, allowing $A_s \approx M_f$. The results verify that the inter-martensitic transformation $A \leftarrow 10M \leftarrow 14M$ is stable up to larger compressive stresses and accounts for significant compressive strain.

When $A \rightarrow 10M$ is bypassed and the transformation steps are $A \rightleftharpoons 14M \rightleftharpoons L1_0$, we observe much wider hysteresis $\Delta T_m \approx \Delta T_h = A_f - M_s$ (right-hand side of Fig. 4b). Apparently, the $10M$ structure promotes fracture and complete recovery is observed because it is bypassed. We will expound on the stress-inducement of $A \rightleftharpoons 14M \rightleftharpoons L1_0$ in the next section; here we consider the contrasting thermal hysteresis when $A \rightleftharpoons 10M \rightleftharpoons 14M$ and $A \rightleftharpoons 14M \rightleftharpoons L1_0$ are stress-induced. Since the DSC results exhibit a small hysteresis for the $A \rightleftharpoons 10M$ transformation, $F_{C(F)}$ should be small for $A \rightleftharpoons 10M \rightleftharpoons 14M$. Furthermore, $10M$ and $14M$ martensite are both monoclinic, making the interface between the two phases highly compatible, which lowers $F_{C(F)}$ as well as $F_{C(R)}$. Based on Eq. (7), the low F_C encourages small temperature hysteresis.

For $A \rightleftharpoons 14M \rightleftharpoons L1_0$, it can be seen in the right-hand side of Fig. 4b that the transformation commences and strain accumulates near 100 °C. Because the temperature greatly exceeds A_f (24.4 °C) determined in the DSC analysis, the austenite is quite resistive to the MT; hence $F_{C(F)}$ probably increases for $A \rightarrow 14M$. The cooling segment is vertical when the temperature decreases by nearly 30 °C. The decrease implies that multiple transforming interfaces grow [17], which increases the interaction energy $W_{\text{interaction(F)}}$. Once $14M \rightarrow L1_0$ introduces the habit plane for $L1_0$, untransformed austenite domains can transform directly to $L1_0$. Micro-scale plasticity may develop because the crystallography of the $14M$ and $L1_0$ structures differ and because $L1_0$ detwins. These factors increase $F_{C(R)}$ and $F_{C(F)}$ in Eqs. (7) and (8) and the hysteresis widens.

We note that the maximum tensile recoverable strains for $A \rightleftharpoons 14M \rightleftharpoons L1_0$ are lower in the ε–T response (+9% in Fig. 4b) compared to the σ–ε response (+12% in Fig. 6b). In compression, on the other hand, the recoverable strains are approximately −6% for both cases (Figs. 5 and 7). The discrepancy results from the large detwinning contribution predicted for the $L1_0$ structure in tension. Apparently, detwinning is curtailed in the ε–T response. This is due to multiple variant interaction as well as the micro-scale plastic deformation discussed in the previous paragraph. Furthermore, the stress drops in the σ–ε response, whereas the high level of stress is constant in ε–T and advances micro-scale plasticity. The large stresses must provide the driving force for single-interface growth when the cooling segment becomes vertical during the transformation to $L1_0$. As a result, the temperature does not change and the transformation is athermal, which is typically associated with miniscule elastic energy storage during growth of a single-interface [17]. As a result, a larger chemical driving force is required for the reverse transformation and A_s increases; therefore high above M_f; $A_s \gg M_s$ and $\Delta T_s > 0$.

5.2. Stress–strain

In the σ–ε response, the stress hysteresis $\Delta\sigma_m$ is smallest when the inter-martensitic transformation $A \rightleftharpoons 10M \rightleftharpoons 14M$ is stress-induced and the $14M$ structure is predominant, analogous to the temperature hysteresis. In compression, a considerable hysteresis is noticeable at $T = 25$ °C even though the transformation $A \rightleftharpoons 10M \rightleftharpoons 14M$ takes place. The initial transformation at $T = 25$ °C is $A \rightarrow 10M$ at the transformation stress, and once the stress increases, $10M$ domains deform while others convert to $14M$. Upon creation of the $14M$ habit plane, $A \rightarrow 14M$ is stress-induced, giving rise to the conspicuous increase in stress observed in Fig. 7. Untransformed $10M$ domains can deform plastically and differently oriented $14M$ variants will grow, and thus F_C and the interaction energy $W_{\text{interaction}}$ increase. These phenomena produce a wider hysteresis according to Eqs. (7) and (8). At $T = 50$ °C, the narrow hysteresis is attributed to the predominance of $A \rightarrow 10M \rightarrow 14M$ and $A \rightarrow 14M$ near the transformation stress.

The intermediate transformation to the $10M$ structure is bypassed and the transformation steps are $A \rightleftharpoons 14M \rightleftharpoons L1_0$ at elevated temperatures (Figs. 6b and 7). The austenite

is stabilized at temperatures greater than A_f. Due to stabilization, larger transformation stresses are required which provide a driving force sufficient to create the $14M$ habit plane directly from austenite. The stress to nucleate the $14M$ phase is less than that required to facilitate the inter-martensitic transformation $14M \rightarrow L1_0$, and the stress reaches a maximum and then drops to a plateau. At the plateau, $A \rightarrow L1_0$ occurs once the habit plane between the austenite and $L1_0$ structure exists. The stress hysteresis increases compared to that for $A \rightleftharpoons 10M \rightleftharpoons 14M$ based on reasoning given for the ε–T analysis.

The inter-martensitic transformation $A \rightleftharpoons 14M \rightleftharpoons L1_0$ is stable at $T \geqslant 50$ °C in tension (Fig. 6b). The hysteresis $\Delta\sigma_m$ decreases due to diminished irreversible contributions attributed to lower detwinning strains. Detwinning is curtailed due to variant interaction (expected at high stresses). In compression, on the other hand, the hysteresis widens. Based on the evolution of the compressive σ–ε response at $T \geqslant 50$ °C (i.e. stress drop, widening hysteresis and slip), we assert the transformation steps evolve as follows: $A \rightleftharpoons 10M \rightleftharpoons 14M$ to $A \rightleftharpoons 14M \rightleftharpoons L1_0$ to $A \rightleftharpoons L1_0$ (see Fig. 7). Based on the rationale provided above, the hysteresis increases because $A \rightleftharpoons L1_0$ becomes the principle transformation. As the initial transformation changes from $A \rightarrow 10M$ to $A \rightarrow L1_0$, the entropy change increases for the different crystal structures, because: (i) the $14M$ and $L1_0$ structures are not the primary thermal-induced structures; and (ii) the $L1_0$ structure is non-modulated and tetragonal, unlike the $10M$ structure. Considering the C–C relation $d\sigma^{tr}/dT = -\Delta s/\varepsilon^{tr}$, it is clear that the compressive transformation stress will increase as well; therefore, a much larger C–C slope is measured in compression (2.75 MPa °C^{-1}) vs. tension (0.36 MPa °C^{-1}) (Fig. 8).

6. Conclusions

To underscore the role of inter-martensitic transformations, we scrutinize both the strain–temperature and stress–strain responses over wide iso-stress and temperature ranges. The present work renders a precise understanding of Ni–Fe–Ga shape memory response and leads to the following conclusions.

1. A close examination of the strain–temperature response during heating and cooling is necessary to distinguish the influences of inter-martensitic transformations in Ni–Fe–Ga. We used a thermo-mechanical formulation to derive theoretical expressions that confirm that the inter-martensitic transformation $A \rightleftharpoons 10M \rightleftharpoons 14M$ enables an A_s temperature below M_s and facilitates narrow hysteresis. Furthermore, the results show $A_s \approx M_f$, which has not, to our knowledge, been observed in previous studies and arises from the differential in the driving forces and strains for the forward $A \rightarrow 10M$ and $A \leftarrow 14M$ reverse inter-martensitic transformations.
2. At temperatures much higher than A_f, and at high transformation stresses, the intermediate $A \rightarrow 10M$ transformation is bypassed, allowing the inter-martensitic transformation $A \rightleftharpoons 14M \rightleftharpoons L1_0$ to occur. In these cases, the intersecting heating and cooling segments are not observed and the hysteresis widens due to irreversibility effects.
3. The inter-martensitic transformation $A \rightleftharpoons 14M \rightleftharpoons L1_0$ is stable at high temperatures in tension and the intermediate transition to $14M$ enables a shallow C–C slope (0.36 MPa °C^{-1}). Therefore the M_d temperature is not observed at temperatures as high as 425 °C. In compression, the evolution of the transformation steps from $A \rightleftharpoons 14M \rightleftharpoons L1_0$ to $A \rightleftharpoons L1_0$ produces a C–C slope (2.75 MPa °C^{-1}) eight times higher, and the M_d temperature appears. Despite this, the pseudoelastic temperature window is still large in compression (275 °C).
4. A significant detwinning contribution (+8.2%) exists for the $L1_0$ structure in tension and facilitates recoverable strains as high as +12% in the σ–ε response. The contribution is curtailed in the ε–T response due to micro-scale plasticity and variant interaction reducing the recoverable strain to +9%. The asymmetry of the recoverable strains in tension vs. compression (−6%) is noteworthy because both cases exhibit excellent recoverability.

Acknowledgements

The work was supported by a Grant CMS -0428428, the National Science Foundation, Division of Civil and Mechanical Systems. The single crystals were obtained from Prof. Y. Chumlyakov of Tomsk State University, Russia.

References

[1] Oikawa K, Ota T, Sutou Y, Ohmori T, Kainuma R, Ishida K. Mate Trans JIM 2002;43:2360.
[2] Li JQ, Liu ZH, Yu HC, Zhang M, Zhou M, Zhou YQ, et al. Solid State Commun 2003;126:323.
[3] Santamarta R, Font J, Muntasell J, Masdeu F, Pons J, Cesari E, et al. Scripta Mater 2006;54:1105.
[4] Murakami Y, Shindo D, Oikawa K, Kainuma R, Ishida K. Appl Phys Lett 2004;85:6170.
[5] Oikawa K, Omori T, Kainuma R, Ishida K. J Mag Mag Mater 2004;272–276:2043.
[6] Omori T, Kamiya N, Sutou Y, Oikawa K, Kainuma R, Ishida K. Mater Sci Eng A 2004;378:403.
[7] Chen F, Meng XL, Cai W, Zhao LC, Wu GH. J. J Mag Mag Mater 2006;302:459.
[8] Sutou Y, Kamiya N, Omori T, Kainuma R, Ishida K, Oikawa K. Appl Phys Lett 2004;84:1275.
[9] Masdeu F, Pons J, Seguí C, Cesari E, Dutkiewicz J. J Magn Magn Mater 2005;290–291:816.
[10] Hamilton RF, Efstathiou C, Sehitoglu H, Chumlyakov Y. Scripta Mater 2006;54:465–9.
[11] Ball JM, James RD. Arch Rat Mech Anal 1987;100:13.
[12] Saburi I, Nenno S. In: Proceedings of the international conference on solid–solid phase transformation, Pittsburgh; 1981. p. 1455.
[13] Gall K, Sehitoglu H. Intl J Plast 1999;15:69.

[14] Niclaeys C, Ben Zineb T, Arbab-Chirani S, Patoor E. Intl J Plast 2002;18:1619.
[15] Ren X, Miura N, Zhang J, Otsuka K, Tanaka K, Koiwa M, et al. Mater Sci Eng A 2001;312:19.
[16] Hamilton RF, Sehitoglu H, Chumlyakov Y, Maier HJ. Acta Mater 2004;52:3383.
[17] Salzbrenner RJ, Cohen M. Acta Metal 1979;27:739.